A&A, 687, L19 (2024)
https://doi.org/10.1051/0004-6361/202449999


Astronomy & Astrophysics

LETTER TO THE EDITOR

# The aspherical explosions of the 03fg-like Type Ia supernovae 2021zny and 2022ilv revealed by polarimetry

T. Nagao[1,2,3], K. Maeda[4], S. Mattila[1,5], H. Kuncarayakti[1,6], C. P. Gutiérrez[7,8], and A. Cikota[9]

[1] Department of Physics and Astronomy, University of Turku, 20014 Turku, Finland
e-mail: t.nagao90@gmail.com
[2] Aalto University Metsähovi Radio Observatory, Metsähovintie 114, 02540 Kylmälä, Finland
[3] Aalto University Department of Electronics and Nanoengineering, PO Box 15500, 00076 Aalto, Finland
[4] Department of Astronomy, Kyoto University, Kitashirakawa-Oiwake-cho, Sakyo-ku, Kyoto 606-8502, Japan
[5] School of Sciences, European University Cyprus, Diogenes Street, Engomi 1516, Nicosia, Cyprus
[6] Finnish Centre for Astronomy with ESO (FINCA), University of Turku, Turku 20014, Finland
[7] Institut d'Estudis Espacials de Catalunya (IEEC), Edifici RDIT, Campus UPC, 08860 Castelldefels (Barcelona), Spain
[8] Institute of Space Sciences (ICE, CSIC), Campus UAB, Carrer de Can Magrans, s/n, 08193 Barcelona, Spain
[9] Gemini Observatory/NSF's NOIRLab, Casilla 603, La Serena, Chile

Received 15 March 2024 / Accepted 1 July 2024

**ABSTRACT**

*Context.* A peculiar subtype of Type Ia supernovae (SNe), 03fg-like (super-Chandrasekhar) SNe, show different observational properties from prototypical Type Ia SNe: they typically have high luminosities at the light-curve peak, low expansion velocities, and strong carbon features. The origin of this class of Type Ia SNe has been actively debated. Recent nebular-phase infrared observations of the 03fg-like Type Ia SN 2022pul using the *James Webb* Space Telescope revealed large-scale asymmetries in the ejecta and the presence of the strong [Ne II] line at 12.81 μm, suggesting a violent merger of two white dwarfs as its origin.
*Aims.* Polarimetry is another powerful tool for studying the overall ejecta asymmetries of spatially unresolved SNe. Here, we aim to check the universality of the violent merger scenario as the origin of 03fg-like Type Ia SNe, by studying their explosion geometries using polarimetry.
*Methods.* In this Letter we present imaging-polarimetric observations of the two 03fg-like Type Ia SNe 2021zny and 2022ilv.
*Results.* SNe 2021zny and 2022ilv show high intrinsic polarization (∼1%–∼2%), which might be composed of multiple components with different polarization angles. This indicates that they have complex aspherical structures in their ejecta, supporting the violent merger scenario for their origin. Our observations provide the first clear evidence from polarimetry for such aspherical structures.

**Key words.** techniques: photometric – supernovae: individual: SN2021zny – supernovae: individual: SN 2022ilv

## 1. Introduction

Type Ia supernovae (SNe) are explosions of white dwarfs (WDs) powered by runaway thermonuclear burning of the degenerate gas (e.g., Maeda & Terada 2016; Livio & Mazzali 2018). Given that the majority of Type Ia SNe show standardizable light-curve (LC) properties, they are popular standard candles for cosmological distance measurements (e.g., Riess et al. 1998; Perlmutter et al. 1999). In addition to such standardizable "normal" Type Ia SNe, it has been recognized that there are subcategories of Type Ia SNe, which show a wide range of photometric and spectroscopic properties (e.g., Taubenberger et al. 2017; Jha et al. 2019). These observational diversities are coupled with different progenitor systems, different evolutionary paths, and/or different thermonuclear burning behavior. However, we have not fully understood the progenitors and explosion mechanisms for different subtypes of Type Ia SNe (e.g., Maoz et al. 2014; Liu et al. 2023).

One extreme subtype is the so-called 03fg-like (or super-Chandrasekhar) Type Ia SN, which shows different observational properties from normal Type Ia SNe (e.g., Howell et al. 2006; Hicken et al. 2007; Scalzo et al. 2010; Yamanaka et al. 2009; Taubenberger et al. 2019; Hsiao et al. 2020; Ashall et al. 2021; Dimitriadis et al. 2023; Srivastav et al. 2023). They are typically brighter, with a peak absolute $B$-band magnitude of $-19 < M_B < -21$ mag (Ashall et al. 2021). In some extreme cases, the required amount of $^{56}$Ni would be similar to the Chandrasekhar mass (∼1.4 $M_\odot$), and they would thus require super-Chandrasekhar-mass WDs as their progenitors, unless other significant energy sources were contributing to their brightness (e.g., Yamanaka et al. 2009). Their LCs evolve slowly, with $\Delta m_{15}(B) < 1.3$ mag, and they have relatively low expansion velocities (8000–12 000 km s$^{-1}$ for Si II $\lambda$6355) and strong features from unburnt carbon in their spectra (Ashall et al. 2021), suggesting more massive SN ejecta compared to normal Type Ia SNe (e.g., Taubenberger et al. 2017).

Several scenarios have been proposed to explain the observational properties of the 03fg-like Type Ia SNe: (1) An explosion of a carbon-oxygen (CO) WD whose mass exceeds the Chandrasekhar limit due to its rapid rotation (e.g., Yoon & Langer 2005) and/or strong magnetic fields (e.g., Das & Mukhopadhyay 2013) formed through the accretion from a non-degenerate companion in the single-degenerate scenario (e.g., Whelan & Iben 1973; Nomoto 1982) or through post-merger accretion in the

double-degenerate scenario (e.g., Iben 1984; Webbink 1984; Raskin et al. 2014). (2) An explosion of a CO WD during a merger with a companion WD (the violent merger scenario; see, e.g., Pakmor et al. 2017, for a review). In this scenario, the high peak luminosity might be due to viewing angle effects of an aspherical explosion (e.g., Hillebrandt et al. 2007; Moll et al. 2014) and/or due to interaction with circumstellar material (CSM; e.g., Hachinger et al. 2012; Noebauer et al. 2016). (3) An explosion after a merger of a WD with the core of a massive asymptotic giant branch star (the core-degenerate scenario; e.g., Sparks & Stecher 1974; Livio & Riess 2003; Kashi & Soker 2011). In this scenario, the high brightness could also be explained by a CSM interaction. Recent, very early-phase observations (within a few days after the explosion) of several 03fg-like SNe have detected early excesses in their LCs, suggesting interaction with H-poor CSM (SNe 2020hvf, 2021zny, 2022ilv, and 2022pul; Jiang et al. 2021; Dimitriadis et al. 2023; Srivastav et al. 2023; Siebert et al. 2024). However, the strength of the CSM interaction estimated from the observed early excesses is not sufficient to boost the peak brightness from the level of normal Type Ia SNe ($\sim -19$ mag) to the observed level in bright 03fg-like SNe ($\sim -20$ mag; e.g., Jiang et al. 2021; Maeda et al. 2023). Therefore, bright 03fg-like SNe still need an additional, stronger CSM interaction or a super-Chandrasekhar mass $^{56}$Ni to explain their extreme brightness.

Nebular-phase observations of the 03fg-like Type Ia SN 2022pul with the *James Webb* Space Telescope exhibited anticorrelated asymmetric emission-line profiles for the iron-group elements (Fe, Co, and Ni) and the intermediate-mass elements (S, Ar, and Ca), as well as the presence of strong [Ne II] at 12.81 µm (Kwok et al. 2024; Siebert et al. 2024). The separate distributions of different elements suggest large global ejecta asymmetries in SN 2022pul and support the violent merger scenario. At the same time, the presence of the strong [Ne II] line was also predicted as a proof of a violent merger scenario by nonlocal-thermodynamic-equilibrium radiative transfer calculations for various scenarios in Type Ia SNe (Blondin et al. 2023). These discoveries on SN 2022pul strongly support the violent merger scenario.

Polarimetry provides another powerful way to study the ejecta geometries of SNe. Its application to the 03fg-like Type Ia SNe has been very limited due to the rareness of this class of SN but can be the key to understanding their origin. Spectropolarimetric observations of the 03fg-like Type Ia SN 2009dc show low continuum polarization (<0.3%) and indicate that the explosion is nearly symmetric (Tanaka et al. 2010). This suggests that the explosion mechanism of SN 2009dc is different from that of SN 2022pul, which showed largely aspherical ejecta. Alternatively, this might merely imply that SN 2009dc had a similarly aspherical explosion but with a different viewing angle (i.e., SN 2009dc might be viewed from a direction close to the axis of symmetry). In fact, an aspherical system is expected for SN 2009dc from the line shapes in the nebular spectra (Siebert et al. 2023). Another example is SN 2007if, which showed relatively high wavelength-independent polarization ($P \sim 0.7$ %, $\theta \sim 130$ degrees) from 13 to 46 days after the brightness peak (Cikota et al. 2019; Chu et al. 2022). Chu et al. (2022) conclude that this polarization likely originates from the interstellar polarization in the Milky Way (MW) as suggested by the relatively high MW extinction, implying that the intrinsic SN polarization is low and thus the explosion should be relatively spherical or viewed from the axis of symmetry. We note that the polarization angle of the observed polarization in SN 2007if is not similar to the directions of the interstellar polarization (ISP) of MW stars or the interstellar magnetic fields in directions near the SN line of sight (~40 degrees; Berdyugin et al. 2014; Bennett et al. 2013), although the local values do not necessarily follow the global values.

In this Letter we present imaging-polarimetric observations of two 03fg-like Type Ia SNe: SNe 2021zny and 2022ilv (Yamanaka 2021; Burke et al. 2022). SN 2021zny showed several characteristics of the class of 03fg-like Type Ia SNe, such as high peak brightness, slow LC evolution, low ejecta velocities, and strong lines from unburnt material (Dimitriadis et al. 2023). Dimitriadis et al. (2023) also report the detection of a flux excess within a few days after the explosion, which can be explained by interaction of the ejecta with $\sim 0.04\,M_\odot$ of CSM at a distance of $\sim 10^{12}$ cm and prominent [O I] $\lambda\lambda$ 6300, 6364 lines at a late phase. From these observational properties, Dimitriadis et al. (2023) conclude that the origin of SN 2021zny is possibly a merger of two CO WDs, where the disrupted secondary WD ejects carbon-rich CSM before the explosion of the primary WD. Srivastav et al. (2023) demonstrate that SN 2022ilv showed similar photometric and spectroscopic features as 03fg-like Type Ia SNe as well as an early excess in the LC, and also proposed a similar merger scenario.

## 2. Observations

We conducted *V*- and *R*-band imaging polarimetry using the Alhambra Faint Object Spectrograph and Camera (ALFOSC)[1] on the 2.56 m Nordic Optical Telescope (NOT[2]) for the 03fg-like Type Ia SNe 2021zny and 2022ilv. The observing logs are shown in Tables 1 and 2. For the linear polarimetry of the SNe, we utilized a half-wave plate (HWP) and a calcite plate. The HWP rotates the polarization axis of the transient light with a certain angle, and then the transient light is split by the calcite plate into two orthogonally polarized beams (the ordinary and extraordinary components). We derived the Stokes parameters from the signals of the ordinary and extraordinary components for four HWP angles (0°, 22.5°, 45°, and 67.5°).

The data were reduced and analyzed with the standard methods (as laid out in, e.g., Patat et al. 2017) using Image Reduction and Analysis Facility (IRAF Tody 1986, 1993). First, we applied the basic treatment (cosmic-ray removal and bias and flat-field corrections) to all the frames. Then, we performed aperture photometry on the ordinary and the extraordinary components of the transient for all the HWP angles. Since the ordinary and extraordinary beams overlap in the ALFOSC images, an artificial polarization signal due to the inhomogeneous structures of the host galaxy and/or the background region can be created. To assess such an error for the polarization, we conducted aperture photometry using four different combinations of the aperture size ($r^{\rm ap}$) and sky region ($r^{\rm sky}$): (1) $r_1^{\rm ap} = 2\times FWHM$, $r_1^{\rm sky} = (2-3)\times FWHM$; (2) $r_2^{\rm ap} = 2\times FWHM$, $r_2^{\rm sky} = (3-4)\times FWHM$; (3) $r_3^{\rm ap} = 2.5\times FWHM$, $r_3^{\rm sky} = (2.5-3.5)\times FWHM$; and (4) $r_4^{\rm ap} = 2.5\times FWHM$, $r_4^{\rm sky} = (3.5-4.5)\times FWHM$, where FWHM denotes the full width at half maximum of the ordinary beam's point-spread function. Based on the measurements from the aperture photometry of the ordinary and extraordinary sources for four different HWP angles, we derived the Stokes $q$ and $u$ values for each combination of the aperture and sky region: $(q_1\pm\sigma_{q,1}, u_1\pm\sigma_{u,1})$, $(q_2\pm\sigma_{q,2}, u_2\pm\sigma_{u,2})$, $(q_3\pm\sigma_{q,3}, u_3\pm\sigma_{u,3})$, and $(q_4\pm\sigma_{q,4}, u_4\pm\sigma_{u,4})$. Here, $\sigma$ represents the photon shot noise.

[1] http://www.not.iac.es/instruments/alfosc/
[2] http://www.not.iac.es

**Table 1.** Imaging-polarimetric observations of SN 2021zny and their measurements.

| Date (UT) | MJD (days) | Phase [(a)] (days) | Exp. time (seconds) | $q_{\rm ave}$ (%) | $u_{\rm ave}$ (%) | Pol. degree (%) | Pol. angle (degree) | Filter |
|---|---|---|---|---|---|---|---|---|
| 2021-10-05.13 | 59492.13 | −6.33 | 4 × 80 | −0.10 ± 0.15 | −0.60 ± 0.18 | 0.56 ± 0.18 | 130.3 ± 3.6 | *V* |
| | | | 4 × 80 | −0.12 ± 0.05 | −0.55 ± 0.14 | 0.53 ± 0.14 | 128.8 ± 1.5 | *R* |
| 2021-10-12.20 | 59499.20 | +0.74 | 4 × 50 | −0.20 ± 0.13 | −0.35 ± 0.10 | 0.37 ± 0.11 | 120.1 ± 4.4 | *V* |
| | | | 4 × 50 | −0.18 ± 0.07 | −0.15 ± 0.13 | 0.19 ± 0.10 | 109.9 ± 6.7 | *R* |
| 2021-11-09.93 | 59527.93 | +29.47 | 4 × 120 | 0.31 ± 0.14 | 0.48 ± 0.31 | 0.44 ± 0.27 | 28.6 ± 5.1 | *V* |
| | | | 4 × 80 | −1.08 ± 0.57 | −1.60 ± 0.24 | 1.86 ± 0.38 | 118.0 ± 3.6 | *R* |
| 2021-11-30.91 | 59548.91 | +50.45 | 4 × 120 | −0.29 ± 0.54 | 0.45 ± 0.37 | 0.19 ± 0.43 | 61.4 ± 13.3 | *V* |
| | | | 4 × 100 | −1.22 ± 0.57 | −0.37 ± 0.52 | 1.02 ± 0.57 | 98.4 ± 5.9 | *R* |

**Notes.** [(a)]Relative to the *B*-band peak: $t_0$ = 59498.46 (MJD; Dimitriadis et al. 2023).

**Table 2.** Imaging-polarimetric observations of SN 2022ilv and their measurements.

| Date (UT) | MJD (days) | Phase [(a)] (days) | Exp. time (seconds) | $q_{\rm ave}$ (%) | $u_{\rm ave}$ (%) | Pol. degree (%) | Pol. angle (degree) | Filter |
|---|---|---|---|---|---|---|---|---|
| 2022-05-03.18 | 59702.18 | -5.28 | 4 × 80 | −1.00 ± 0.03 | 1.50 ± 0.07 | 1.80 ± 0.06 | 61.8 ± 0.4 | *V* |
| | | | 4 × 80 | −0.97 ± 0.11 | 1.88 ± 0.15 | 2.11 ± 0.144 | 58.6 ± 0.8 | *R* |
| 2022-05-14.00 | 59713.00 | +5.54 | 4 × 80 | −1.57 ± 0.19 | 1.95 ± 0.07 | 2.50 ± 0.13 | 64.4 ± 0.9 | *V* |
| | | | 4 × 80 | 40.14 ± 0.57 | 1.16 ± 0.40 | 1.03 ± 0.40 | 41.6 ± 7.0 | *R* |
| 2022-06-03.95 | 59733.95 | +26.49 | 4 × 100 | −1.27 ± 0.17 | 1.26 ± 0.30 | 1.76 ± 0.24 | 67.6 ± 2.0 | *V* |
| | | | 4 × 100 | 4 − 1.14 ± 0.08 | 0.64 ± 0.11 | 1.30 ± 0.09 | 75.3 ± 1.1 | *R* |
| 2022-06-26.96 | 59756.96 | +49.50 | 4 × 120 | −1.57 ± 0.09 | 0.29 ± 0.20 | 1.59 ± 0.10 | 84.8 ± 1.8 | *V* |
| | | | 4 × 100 | −1.23 ± 0.19 | 1.83 ± 0.58 | 2.09 ± 0.49 | 62.0 ± 2.3 | *R* |
| 2022-07-07.94 | 59767.94 | +60.48 | 4 × 120 | 0.55 ± 0.45 | 0.49 ± 0.16 | 0.57 ± 0.35 | 20.8 ± 6.3 | *V* |
| | | | 4 × 120 | 0.35 ± 0.66 | 1.49 ± 0.99 | 0.91 ± 0.98 | 38.4 ± 6.4 | *R* |

**Notes.** [(a)]Relative to the *g*-band peak: $t_0$ = 59707.46 (MJD; Srivastav et al. 2023).

Then, we took the average and standard deviation of these $q$ and $u$ values as the polarization signal and the error, respectively:

$$q_{\rm ave} = \frac{\Sigma_{i=1}^{n}\left(\frac{q_i}{\sigma_{q,i}^2}\right)}{\Sigma_{i=1}^{n}\left(\frac{1}{\sigma_{q,i}^2}\right)}, \sigma_{q,\rm ave} = \sqrt{\frac{\Sigma_{i=1}^{n}\left(\frac{1}{\sigma_{q,i}^2}\right)(q_i - q_{\rm ave})^2}{(n-1)\Sigma_{i=1}^{n}\left(\frac{1}{\sigma_{q,i}^2}\right)}}, \quad (1)$$

$$u_{\rm ave} = \frac{\Sigma_{i=1}^{n}\left(\frac{u_i}{\sigma_{u,i}^2}\right)}{\Sigma_{i=1}^{n}\left(\frac{1}{\sigma_{u,i}^2}\right)}, \sigma_{u,\rm ave} = \sqrt{\frac{\Sigma_{i=1}^{n}\left(\frac{1}{\sigma_{u,i}^2}\right)(u_i - u_{\rm ave})^2}{(n-1)\Sigma_{i=1}^{n}\left(\frac{1}{\sigma_{u,i}^2}\right)}}. \quad (2)$$

Here, $n$ is the number of the measurements to be averaged and $n$ = 4. From these averaged $q$ and $u$ values, we calculated the polarization degree and the polarization angle:

$$P = \sqrt{q_{\rm ave}^2 + u_{\rm ave}^2}, \quad (3)$$

$$\sigma_P = \sqrt{\left(\frac{\partial P}{\partial q_{\rm ave}}\sigma_{q,\rm ave}\right)^2 + \left(\frac{\partial P}{\partial u_{\rm ave}}\sigma_{u,\rm ave}\right)^2}$$

$$= \sqrt{\left(\frac{q_{\rm ave}}{P}\sigma_{q,\rm ave}\right)^2 + \left(\frac{u_{\rm ave}}{P}\sigma_{u,\rm ave}\right)^2}, \quad (4)$$

$$\chi = \frac{1}{2}\arctan\left(\frac{u_{\rm ave}}{q_{\rm ave}}\right), \quad (5)$$

$$\sigma_\chi = \sqrt{\left(\frac{\partial \chi}{\partial q_{\rm ave}}\sigma_{q,\rm ave}\right)^2 + \left(\frac{\partial \chi}{\partial u_{\rm ave}}\sigma_{u,\rm ave}\right)^2}$$

$$= \frac{\sqrt{\left(u_{\rm ave}\sigma_{q,\rm ave}\right)^2 + \left(q_{\rm ave}\sigma_{u,\rm ave}\right)^2}}{2P^2}. \quad (6)$$

Finally, we subtracted the polarization bias from the polarization degrees following the standard method laid out in Wang et al. (1997).

## 3. Results and discussion

Figure 1 shows the time evolution of the *V*- and *R*-band polarization of SN 2021zny. Both the *V*- and *R*-band polarization show $P \sim 0.4$ % and $\theta \sim 120$ degrees around the peak. At Phase +29.47 days, the degree of the *R*-band polarization increased to ∼1.9 % and the polarization angle remained at around ∼120 degrees; the polarization degree and angle both fell slightly at Phase +50.45 days. On the other hand, the *V*-band polarization at Phases +29.47 and +50.45 days shows small degrees of polarization ($\lesssim$0.5 %) with different polarization angles (∼45 degrees) from ∼120 degrees around the peak. The polarization is also shown in the $q - u$ plane (Fig. 2).

The SN can have not only intrinsic polarization but also ISP. Dimitriadis et al. (2023) estimated the total dust extinction in the MW and in the host galaxy to be $E(B-V)_{\rm tot} = 0.14 \pm 0.07$ mag for SN 2021zny. The empirical relation from Serkowski et al. (1975) indicates that its ISP should likely have $P_{\rm max} \lesssim 1.3$ %.

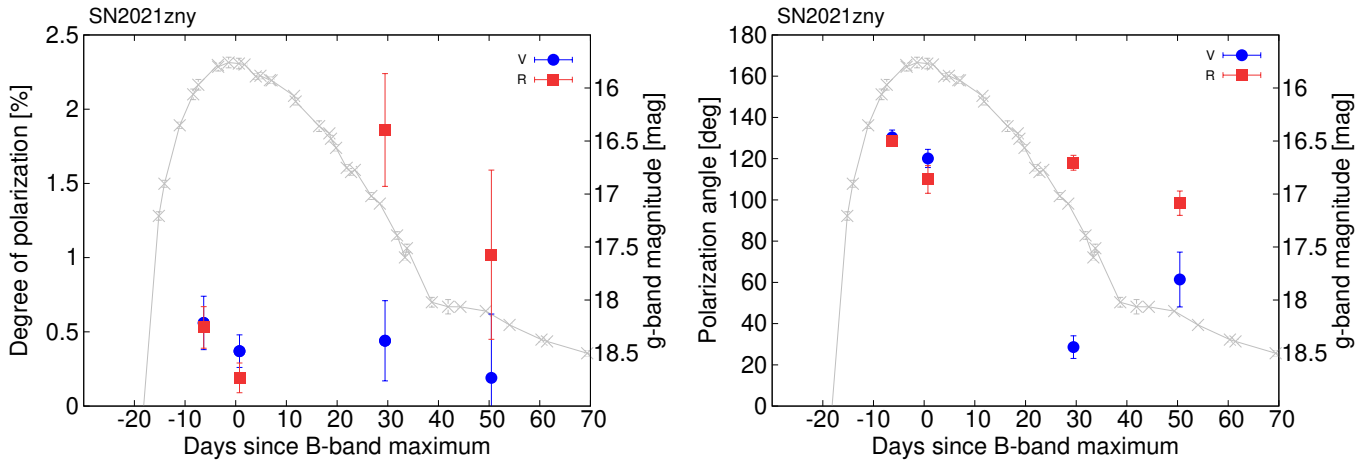


**Fig. 1.** Polarization degree and angle of the $V$- (blue circle) and $R$-band (red square) polarization in SN 2021zny. The gray crosses connected with lines show the $g$-band LC of SN 2021zny from Dimitriadis et al. (2023).

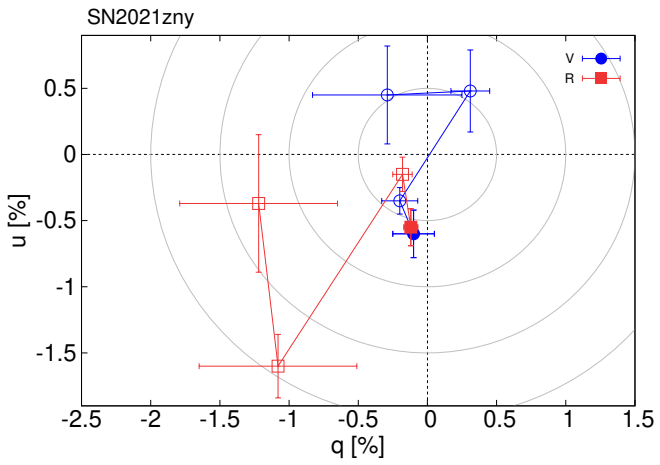


**Fig. 2.** Time evolution of the $V$- (blue) and $R$-band (red) polarization in SN 2021zny in the $q - u$ plane. The first-epoch data (Phase −6.33 days) are shown with filled points. The gray lines correspond to the polarization degrees of 0.5, 1.0 and 1.5 % from the origin, respectively.

From the values of the polarization degree, the polarization component whose angle is ∼ 45 degrees (the $V$-band polarization at Phases +29.47 and +50.45 days) can be explained as being due to the ISP. This interpretation may naturally explain the discrepancy between the $V$- and $R$-band polarization at Phases +29.47 and +50.45 days. The $V$-band polarization shows the ISP due to the line depolarization of the strong continuum polarization, while the $R$-band polarization reflects the strong continuum polarization. Alternatively, the $V$-band polarization shows the ISP due to the low intrinsic SN continuum polarization, while the $R$-band polarization shows a strong line polarization. In this case, the axis of the aspherical distribution of the elements for the strong line polarization should be the same as that of the overall ejecta geometry predicted by the continuum polarization at the first two phases. We note that the directions of the magnetic fields, which are supposed to be aligned with the ISP angle (e.g., Davis & Greenstein 1951), tend to follow the directions of the spiral arms in a spiral galaxy (e.g., Beck 2015). Therefore, the polarization angle of this component ($\theta \sim 45$ degrees), which nicely corresponds to the structure of the host galaxy (see Fig. 1 in Dimitriadis et al. 2023), might support this interpretation. Adopting this component ($P \sim 0.3$ % and $\chi \sim 45$ degrees) as the ISP, the $V$- and $R$-band polarization both show ∼1.0 % of the intrinsic polarization around the brightness peak and then ∼0 and ∼2.0 %, respectively, at a later phase. Even if this component is another component of the intrinsic SN polarization and the ISP is negligible, the intrinsic polarization is high (∼1 – ∼2%), at the highest end of the range of Type Ia SN polarization, or possibly beyond ($\lesssim$1 %; e.g.,Cikota et al. 2019). This indicates that the ejecta of SN 2021zny is significantly aspherical, even compared to the extreme cases of normal Type Ia SNe.

There is another possibility for the origin of the continuum polarization in Type Ia SNe: the polarization due to the scattering by circumstellar dust (e.g., Nagao et al. 2018; Hu et al. 2022). The polarization created by this mechanism depends on the wavelength (typically a higher polarization in bluer wavelengths) and the time (typically a higher polarization at the beginning of the tail phase than at the peak), as demonstrated in Nagao et al. (2018). There are some observational examples (e.g., Yang et al. 2018). Firstly, the polarization in SN 2021zny does not show a clear wavelength dependence at Phases +29.47 or +50.45 days, while it shows higher degrees in the $R$ band than those in the $V$ band at a later phase. Secondly, SN 2021zny already shows relatively high polarization degrees before the B-band peak (∼0.4 % at Phase –6.33). These features cannot be explained with the dust scattering scenario. Therefore, we reject the possibility of scattering in circumstellar dust as the origin of the polarization in SN 2021zny.

Figure 3 shows the time evolution of the $V$- and $R$-band polarization in SN 2022ilv. The polarization degrees are high and time-variable around ∼2.0 % with a relatively constant polarization angle of around ∼60 degrees, except for the data at Phase +60.48 days ($P \sim 0.5$ %, $\theta \sim 30$ degrees). The polarization degrees and angles in the $V$ and $R$ bands are relatively consistent at all phases except Phase +5.54, indicating wavelength-independent polarization (i.e., continuum polarization rather than line polarization). The polarization at Phase +5.54 may be due to the effects of line polarization and depolarization. This polarization behavior is also seen in the $q - u$ plane (Fig. 4), although the early-phase points are clustered around a point that deviates from the points at Phase +60.48 days, except the $R$-band point at Phase +5.54.

Srivastav et al. (2023) estimated the dust extinction for SN 2022ilv to be $E(B - V)_{\rm tot} = 0.11$ mag, assuming that the extinction arises only from the MW dust because the host galaxy is extremely faint and thus should have a low metallicity and a

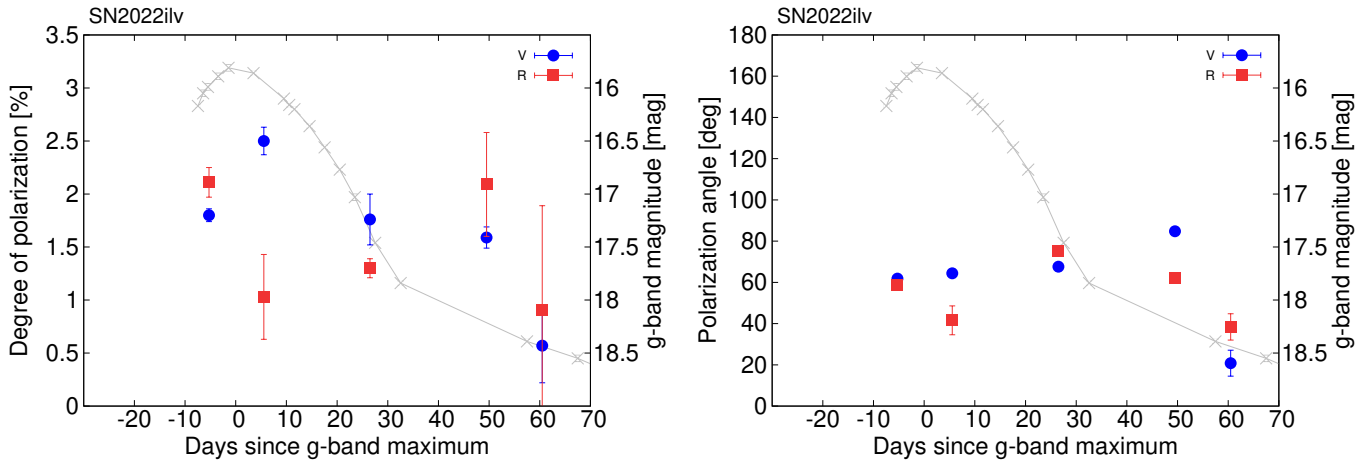


**Fig. 3.** Same as Fig. 1 but for SN 2022ilv. The gray dots connected with lines show the $g$-band LC of SN 2022ilv from Srivastav et al. (2023).

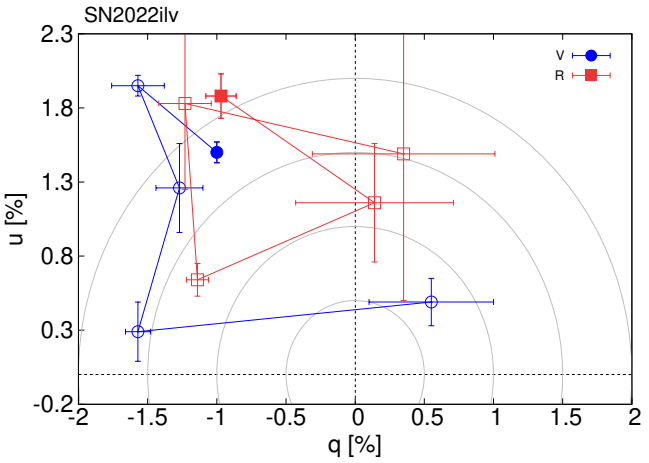


**Fig. 4.** Same as Fig. 2 but for SN 2022ilv. The gray lines correspond to the polarization degrees of 0.5, 1.0, 1.5, and 2.0 % from the origin, respectively.

small amount of dust. Adopting this value, the empirical relation from Serkowski et al. (1975) indicates that its ISP should have $P_{\rm max} \lesssim 1.0$ %. Given that the observed polarization around the peak is too high to be dominated by the ISP, it should be dominated by the intrinsic SN polarization. The polarization degrees at Phase +60.48 days can be consistent with the ISP. However, the polarization angle of the ISP in the MW along the line of sight to SN 2022ilv is estimated to be ∼130 degrees from polarimetric observations of MW stars at ∼100−∼600 pc (Fig. 3 in Berdyugin et al. 2014). Given that the MW extinction for SN 2022ilv is mainly caused by dust at ≲140 pc (Green et al. 2019), the maximum ISP can be estimated to be ≲1.0 and the average value to be ∼0.5% (Fig. 4 in Berdyugin et al. 2014). Therefore, we conclude that the ISP is negligible (≲0.5%) and that the polarization at Phase +60.48 days might still indicate another intrinsic component with a slightly different angle ($P \sim 0.5$ %, $\theta \sim 30$ degrees), in addition to the intrinsic component at the early phases (∼2.0% and ∼60 degrees). This might indicate inhomogeneous structures in the SN ejecta. Even if we assume that the polarization at Phase +60.48 days is dominated by the ISP, the ISP-subtracted intrinsic SN polarization at early phases is high ($P \sim 2.0$%). As in the case of SN 2021zny, the polarization in SN 2021ilv cannot be explained by the scattering in circumstellar dust either. In any case, the intrinsic SN polarization is very high, ∼2%, which is the highest intrinsic continuum polarization observed in any Type Ia SN (e.g., Wang & Wheeler 2008; Cikota et al. 2019). This implies that the ejecta of SN 2022ilv is also highly aspherical compared to any other Type Ia SN.

The degrees of the $V$- and $R$-band polarization in SNe 2021zny and 2022ilv are high (∼1 − ∼2%), indicating large aspherical structures. According to the numerical calculations of the polarization signal in various scenarios for Type Ia SNe by Bulla et al. (2016b,a), the only possible scenario that would explain such a high polarization (i.e., a large aspherical structure) is the violent merger scenario. While several different modes of observations have suggested there are aspherical structures in the 03fg-like Type Ia SNe (see Sect. 1), our observations provide the first evidence from polarimetry.

*Acknowledgements.* We thank Masayuki Yamanaka for helpful discussions. This work is based on observations made under program IDs P64-023, P65-004 and P65-005 with the Nordic Optical Telescope, owned in collaboration by the University of Turku and Aarhus University, and operated jointly by Aarhus University, the University of Turku and the University of Oslo, representing Denmark, Finland and Norway, the University of Iceland and Stockholm University at the Observatorio del Roque de los Muchachos, La Palma, Spain, of the Instituto de Astrofisica de Canarias. TN acknowledges support from the Research Council of Finland projects 324504, 328898 and 353019. KM acknowledges support from the Japan Society for the Promotion of Science (JSPS) KAKENHI grant (JP20H00174 and JP24H01810) and by the JSPS Open Partnership Bilateral Joint Research Project between Japan and Finland (JPJSBP120229923). S. M. was funded by the Research Council of Finland project 350458. HK was funded by the Research Council of Finland projects 324504, 328898, and 353019. CPG acknowledges financial support from the Secretary of Universities and Research (Government of Catalonia) and by the Horizon 2020 Research and Innovation Programme of the European Union under the Marie Skłodowska-Curie and the Beatriu de Pinós 2021 BP 00168 programme, from the Spanish Ministerio de Ciencia e Innovación (MCIN) and the Agencia Estatal de Investigación (AEI) 10.13039/501100011033 under the PID2020-115253GA-I00 HOSTFLOWS project, and the program Unidad de Excelencia María de Maeztu CEX2020-001058-M.

## References

Ashall, C., Lu, J., Hsiao, E. Y., et al. 2021, ApJ, 922, 205
Beck, R. 2015, A&A Rv., 24, 4
Bennett, C. L., Larson, D., Weiland, J. L., et al. 2013, ApJS, 208, 20
Berdyugin, A., Piirola, V., & Teerikorpi, P. 2014, A&A, 561, A24
Blondin, S., Dessart, L., Hillier, D. J., Ramsbottom, C. A., & Storey, P. J. 2023, A&A, 678, A170
Bulla, M., Sim, S. A., Kromer, M., et al. 2016a, MNRAS, 462, 1039
Bulla, M., Sim, S. A., Pakmor, R., et al. 2016b, MNRAS, 455, 1060

Burke, J., Howell, D. A., McCully, C., et al. 2022, Transient Name Server Classification Report, 2022–1137, 1
Chu, M. R., Cikota, A., Baade, D., et al. 2022, MNRAS, 509, 6028
Cikota, A., Patat, F., Wang, L., et al. 2019, MNRAS, 490, 578
Das, U., & Mukhopadhyay, B. 2013, Phys. Rev. Lett., 110, 071102
Davis, L. J., & Greenstein, J. L. 1951, ApJ, 114, 206
Dimitriadis, G., Maguire, K., Karambelkar, V. R., et al. 2023, MNRAS, 521, 1162
Green, G. M., Schlafly, E., Zucker, C., Speagle, J. S., & Finkbeiner, D. 2019, ApJ, 887, 93
Hachinger, S., Mazzali, P. A., Taubenberger, S., et al. 2012, MNRAS, 427, 2057
Hicken, M., Garnavich, P. M., Prieto, J. L., et al. 2007, ApJ, 669, L17
Hillebrandt, W., Sim, S. A., & Röpke, F. K. 2007, A&A, 465, L17
Howell, D. A., Sullivan, M., Nugent, P. E., et al. 2006, Nature, 443, 308
Hsiao, E. Y., Hoeflich, P., Ashall, C., et al. 2020, ApJ, 900, 140
Hu, M., Wang, L., & Wang, X. 2022, ApJ, 931, 110
Iben, I., & J. & Tutukov, A. V., 1984, ApJS, 54, 335
Jha, S. W., Maguire, K., & Sullivan, M. 2019, Nat. Astron., 3, 706
Jiang, J.-A., Maeda, K., Kawabata, M., et al. 2021, ApJ, 923, L8
Kashi, A., & Soker, N. 2011, MNRAS, 417, 1466
Kwok, L. A., Siebert, M. R., Johansson, J., et al. 2024, ApJ, 966, 135
Liu, Z.-W., Röpke, F. K., & Han, Z. 2023, RAA, 23, 082001
Livio, M., & Mazzali, P. 2018, Phys. Rep., 736, 1
Livio, M., & Riess, A. G. 2003, ApJ, 594, L93
Maeda, K., & Terada, Y. 2016, Int. J. Mod. Phys. D, 25, 1630024
Maeda, K., Jiang, J.-A., Doi, M., Kawabata, M., & Shigeyama, T. 2023, MNRAS, 521, 1897
Maoz, D., Mannucci, F., & Nelemans, G. 2014, ARA&A, 52, 107
Moll, R., Raskin, C., Kasen, D., & Woosley, S. E. 2014, ApJ, 785, 105
Nagao, T., Maeda, K., & Yamanaka, M. 2018, MNRAS, 476, 4806
Noebauer, U. M., Taubenberger, S., Blinnikov, S., Sorokina, E., & Hillebrandt, W. 2016, MNRAS, 463, 2972
Nomoto, K. 1982, ApJ, 253, 798
Pakmor, R. 2017, in Handbook of Supernovae, eds. A. W. Alsabti, & P. Murdin, 1257
Patat, F. 2017, in Handbook of Supernovae, eds. A. W. Alsabti, & P. Murdin, 1017
Perlmutter, S., Aldering, G., Goldhaber, G., et al. 1999, ApJ, 517, 565
Raskin, C., Kasen, D., Moll, R., Schwab, J., & Woosley, S. 2014, ApJ, 788, 75
Riess, A. G., Filippenko, A. V., Challis, P., et al. 1998, AJ, 116, 1009
Scalzo, R. A., Aldering, G., Antilogus, P., et al. 2010, ApJ, 713, 1073
Serkowski, K., Mathewson, D. S., & Ford, V. L. 1975, ApJ, 196, 261
Siebert, M. R., Foley, R. J., Zenati, Y., et al. 2023, ApJ, 958, 173
Siebert, M. R., Kwok, L. A., Johansson, J., et al. 2024, ApJ, 960, 88
Sparks, W. M., & Stecher, T. P. 1974, ApJ, 188, 149
Srivastav, S., Smartt, S. J., Huber, M. E., et al. 2023, ApJ, 943, L20
Tanaka, M., Kawabata, K. S., Yamanaka, M., et al. 2010, ApJ, 714, 1209
Taubenberger, S. 2017, in Handbook of Supernovae, eds. A. W. Alsabti, & P. Murdin, 317
Taubenberger, S., Floers, A., Vogl, C., et al. 2019, MNRAS, 488, 5473
Tody, D. 1986, SPIE Conf. Ser., 627, 733
Tody, D. 1993, ASP Conf. Ser., 52, 173
Wang, L., & Wheeler, J. C. 2008, ARA&A, 46, 433
Wang, L., Wheeler, J. C., & Höflich, P. 1997, ApJ, 476, L27
Webbink, R. F. 1984, ApJ, 277, 355
Whelan, J., & Iben, I. J. 1973, ApJ, 186, 1007
Yamanaka, M. 2021, Transient Name Server Classification Report, 2021–3361, 1
Yamanaka, M., Kawabata, K. S., Kinugasa, K., et al. 2009, ApJ, 707, L118
Yang, Y., Wang, L., Baade, D., et al. 2018, ApJ, 854, 55
Yoon, S. C., & Langer, N. 2005, A&A, 435, 967